Article:

Decker, Zachary, Zarzana, Kyle J., Coggon, Matthew et al. (15 more authors) (2019) Nighttime chemical transformation in biomass burning plumes:A box model analysis initialized with aircraft observations. Environmental Science and Technology. pp. 2529-2538. ISSN 1520-5851

https://doi.org/10.1021/acs.est.8b05359

Supporting Information for Nighttime chemical transformation in biomass burning plumes: a box model analysis initialized with aircraft observations

Zachary C. J. Decker[1,2,3], Kyle J. Zarzana[1,2,3], Matthew Coggon[1,3], Kyung-Eun Min[1,3,†], Ilana Pollack[1,††], Thomas B. Ryerson[3], Jeff Peischl[1,3], Pete Edwards[4], William P. Dubé[1,3], Milos Z. Markovic[1,†††], James M. Roberts[1,3], Patrick R. Veres[3], Martin Graus[1,††††], Carsten Warneke[1,3], Joost de Gouw[1,2], Lindsay E. Hatch[5], Kelley C. Barsanti[5], Steven S. Brown[2,3,]*

[1]Cooperative Institute for Research in Environmental Sciences, University of Colorado, Boulder, Colorado, 80309, United States. [2]Department of Chemistry, University of Colorado, Boulder, Colorado 80309-0215, United States. [3]NOAA Earth System Research Laboratory (ESRL), Chemical Sciences Division, Boulder, Colorado 80305, United States. [4]Wolfson Atmospheric Chemistry Laboratories, Department of Chemistry, University of York, York YO10 5DD, United Kingdom. [5]Department of Chemical and Environmental Engineering and College of Engineering – Center for Environmental Research and Technology (CE-CERT), University of California, Riverside, California 92507, United States. [†]Now at Gwangju Institute of Science and Technology, School of Earth Sciences and Environmental Engineering, Gwangju, South Korea 61005. [††]Now at Colorado State University, Atmospheric Science Department, Ft. Collins, CO, USA 80523-1371. [†††]Now at Picarro inc, Santa Clara, CA, 95054. [††††]Now at the Department of Atmospheric and Cryospheric Sciences, University of Innsbruck, Austria 6020.

* steven.s.brown@noaa.gov

Abstract: Biomass burning (BB) is a large source of reactive compounds to the atmosphere. While the daytime photochemistry of BB emissions has been studied in some detail, there has been little focus on nighttime reactions despite the potential for substantial oxidative and heterogeneous chemistry. Here we present the first analysis of nighttime aircraft intercepts of agricultural BB plumes using observations from the NOAA WP-3D aircraft during the 2013 Southeast Nexus (SENEX) campaign. We use these observations in conjunction with detailed chemical box modeling to investigate the formation and fate of oxidants (NO_3, N_2O_5, O_3, and OH) and BB volatile organic compounds (BBVOCs), using emissions representative of agricultural burns (rice straw) and western wildfires (ponderosa pine). Field observations suggest NO_3 production was approximately 1 ppbv hr^{-1}, while NO_3 and N_2O_5 were at or below 3 pptv, indicating rapid NO_3/N_2O_5 reactivity. Model analysis shows that >99% of NO_3/N_2O_5 loss is due to BBVOC + NO_3 reactions rather than aerosol uptake of N_2O_5. Nighttime BBVOC oxidation for rice straw and ponderosa pine fires is dominated by NO_3 (72, 53%, respectively) but O_3 oxidation is significant (25, 43%) leading to roughly 55% overnight depletion of the most reactive BBVOCs and NO_2.

Introduction

Wildfire size and frequency in the Western U.S. has increased over the last 20 years, and these trends are projected to continue due to factors such as forest management practices, elevated summer temperatures, earlier snowmelt, and drought.[1,2] Biomass burning (BB), including wildfires, prescribed burning, and agricultural burning, represents a large, imperfectly characterized and chemically complex source of reactive material to the troposphere. BB releases reactive species and particulate matter that impact the radiative balance of the atmosphere, air quality, and human health on local to global scales.[3–7] The gas-phase components of BB plumes include volatile organic compounds (BBVOCs) as well as nitrogen oxides (NO_x=NO+NO_2 and higher oxides such as peroxyacyl and alkyl nitrates), oxidants, and oxidant precursors. The air quality and climate effects of BB emissions are defined in part by the oxidative processes and atmospheric chemical cycles that occur as the smoke is transported, diluted, and exposed to oxidants over the hours and weeks following emission.

The photochemistry of BB plumes has been studied previously in a number of field and laboratory studies. Daytime BB plumes can have OH concentrations 5-10 times higher than background air[8] and daytime reactions of NO_x, BBVOCs, and OH involve complex pathways that generally lead to O_3 formation, but in some cases to near-field O_3 titration.[9–14] Much less is known about nighttime BB plume oxidative processes, which are expected to be dominated by nitrate radicals (NO_3) and O_3.[15] NO_3 is formed by O_3 oxidation of NO_x (R1 & Figure 1) but is rapidly (τ < 10 s) destroyed in the daytime by NO and photolysis.[15,16] NO_3 is a precursor for N_2O_5 (R2), a NO_x reservoir. N_2O_5 may undergo heterogeneous uptake to form $ClNO_2$ and HNO_3 (R3). The former is a daytime Cl radical precursor affecting both marine and continental environments and influencing next-day O_3 production.[17–20] NO_3 can also be directly taken up onto aerosol (R4).

$$NO_2 + O_3 \rightarrow NO_3 \quad \text{(R1)}$$

$$NO_3 + NO_2 \rightleftharpoons N_2O_5 \quad \text{(R2)}$$

$$N_2O_{5\,(g)} + aerosol \rightarrow \phi ClNO_2 + (2-\phi)HNO_3 \quad \text{(R3)}$$

$$NO_3 + aerosol \rightarrow Products \quad \text{(R4)}$$

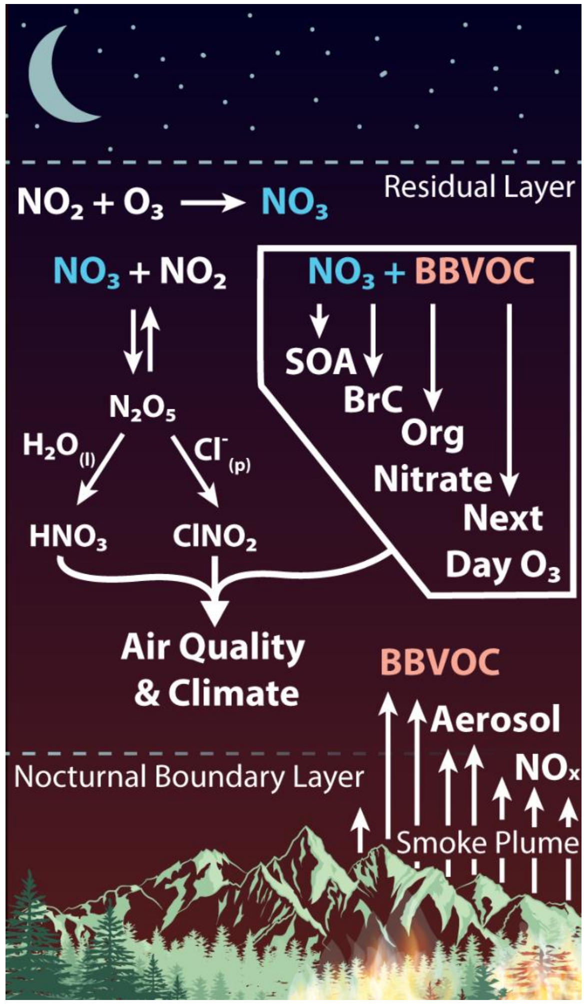

Figure 1. Schematic of nighttime NO_3 and N_2O_5 chemical processing in a biomass burning plume.

Mixing of background or smoke-derived[14] O_3 with NO_x in a BB plume leads to the production of NO_3, which may be rapid (>0.5 ppbv hr^{-1}). Recent laboratory measurements conducted during both the Fire Lab at Missoula Experiment (FLAME-4) and the on-going Fire Influence on Regional and Global Environments Experiment (FIREX) have provided detailed identification and quantification of emissions for a range of BBVOCs.[4,5,21–23] Emissions inventories from these experiments indicate that the compounds emitted and their relative concentrations depend on the fuel type (e.g., pine vs. grass), combustion process (e.g., smoldering or flaming), ignition procedure (fast or slow), and pyrolysis temperature (e.g., high or low).[4,21,24,25] Generally, primary BBVOC emissions include oxygenated hydrocarbons and aromatics (e.g., phenols), as well as unsaturated hydrocarbons, biogenic and hetero-aromatic species.[4,5,21] Many such compounds are very reactive toward NO_3[26–33] and may significantly limit its lifetime, promote secondary organic aerosol formation (SOA)[34,35], and alter nighttime oxidative budgets.

The co-emission of NO_x, highly reactive VOCs, and aerosol particles leads to the potential for significant nighttime chemical transformations. Despite this potential, there has been only one aircraft campaign to date from which sampling of nighttime biomass burning plumes has been reported.[36,37] The Southeast Nexus (SENEX) campaign in 2013 included 20 research flights of an instrumented NOAA WP-3D aircraft and one of the goals was to study the interactions between anthropogenic and biogenic emissions.[38] A night flight on July 2-3 targeted the emissions and nighttime chemistry from a power plant plume near the Mississippi river. During this flight the WP-3D also targeted and intercepted agricultural BB plumes yielding the first airborne study of nighttime smoke that included NO_3 and N_2O_5 measurements.[36] Even so there has been no previous analysis of BB NO_3 chemistry using nighttime aircraft intercepts.

Here, we present the first analysis of nighttime smoke oxidation based on aircraft intercepts of fire plumes using data from this flight. With these observations we initiate a detailed chemical box model to understand the chemical evolution of oxidants (NO_3, N_2O_5, O_3, and OH) and BBVOCs over one night (10 hours) using emissions for rice straw to model a generic agricultural burning plume. We then use this analysis to model nighttime chemistry in western wildfires using emissions for a ponderosa pine fire.

Field and Laboratory Measurements

Field data for this study were taken from multiple instruments deployed on the NOAA WP-3D aircraft during the SENEX 2013[38] flight on July 2-3, 2013 (20:00-03:00 CDT). Our analysis utilizes data from the NOAA nitrogen oxide cavity ring-down spectrometer (CRDS) for NO_2, NO_3, N_2O_5, and O_3,[39–42] as well as the NO_yO_3 chemiluminescence instrument (CL) for NO, NO_2, O_3, and NO_y[43] with 1 Hz acquisition resolution. Within the plume regions we study, the measurements of NO_2 and O_3 from the CRDS and CL instruments agree within 7%. We also use data from an ultra-high sensitivity aerosol spectrometer (UHSAS) for aerosol size measurements (1Hz) [44,45] and a proton-transfer-reaction mass spectrometer (PTR-MS) for VOC measurements (1 s every 17 s)[46].

BB intercepts were identified by the enhancement above background of four species: black carbon (BC), glyoxal (CHOCHO), CO, and acryloyl peroxynitrate (APAN).[36,47] BB identifier data were provided by the NOAA airborne cavity enhanced spectrometer (ACES)[48] for glyoxal, iodide chemical ionization mass spectrometer (I^- CIMS) for APAN[49], single particle soot photometer (SP2) for black carbon[50], and vacuum ultra-violet fluorimeter for CO[51]. Power plant plumes were identified by above background enhancements of NO_x and N_2O_5. While CO is also present in the power plant plumes, the three other BB identifiers were not. Information on background and plume measurements are in the SI (Table S1 & S2).

Five VOCs (toluene, isoprene + furan, methylvinylketone + methacrolein (MVK+MACR), and methylethylketone (MEK)) as well as acetonitrile were measured by the PTR-MS during SENEX and overlap with our inventory. However, we explain in the SI that we do not use these observations because we do not know the fire source, number of fires, or fuel and plume age estimates are highly uncertain (Figure S5).

Our detailed chemical box model uses emission inventories from Hatch et al.[5] and Koss et al.[4] for the ponderosa pine and rice straw fuels. The BBVOC emissions from Hatch et al.[5,21] were measured during FLAME-4 using the following instruments: two-dimensional gas chromatography–time-of-flight mass spectrometry, open-path Fourier-transform infrared spectroscopy[22], whole-air sampling with one-dimensional gas chromatography–mass spectrometry, and PTR time-of-flight mass spectrometry (PTR-ToF)[52]. BBVOC emissions from Koss et al.[4] were measured by PTR-ToF during FIREX. Details regarding how the two inventories were merged is included in the SI. In general, for compounds shared between both inventories, the emission ratios (E1) agree within an order of magnitude with some exceptions (Figure S6). We propagate this variability into our model results (SI).

Analysis and Modeling Methods

We report our emissions in the form of laboratory-derived emission ratios (ER), which is the background subtracted emitted compound (x) normalized to background subtracted CO.[4,21]

$$ER_x = \frac{x\ (ppbv)}{CO(ppmv)} \quad \text{(E1)}$$

These emissions are integrated over the entirety of the laboratory fires and therefore contain emissions from all stages of the fire.

The modified combustion efficiency (MCE) was calculated for each plume.

$$MCE = \frac{CO_2 - CO_{2_{bkg}}}{\left(CO_2 - CO_{2_{bkg}}\right) + (CO - CO_{bkg})} \quad \text{(E2)}$$

During plume intercepts, the average MCE was 95 $\pm$ 6%, which is consistent with previous MCE calculations of the July 2/3 night flight.[36]

Total NO_3 reactivity toward BBVOCs is given by

$$k_{NO_3}^{BBVOC} = \sum k_{NO_3+BBVOC_i}[BBVOC_i] \quad \text{(E3)}$$

where $k_{NO_3+BBVOC_i}$ is the bimolecular rate coefficient for NO_3 + $BBVOC_i$ and $k_{NO_3}^{BBVOC}$ is the pseudo-first order rate coefficient. The bimolecular rate coefficients for NO_3, O_3, or OH + BBVOC were taken from literature where available and estimated by structure activity relationships[31,53] or structural similarity where unavailable (SI).

Due to limited literature on NO_3 + BBVOC rate coefficients, our inventory excludes many nitriles, amines, alkynes, acids, and other compounds whose rate coefficients were unavailable and could not be estimated. We also removed saturated hydrocarbons because they are generally unreactive toward NO_3.[28] Despite this, our merged inventory retains about 87% of the total inventory carbon mass, or 96% by mass, with 235 compounds from Hatch et al.[5] and 171 compounds from Koss et al.[4] with 103 compounds shared in both inventories for a total of 303 unique compounds.

To calculate the observed NO_3 reactivity during SENEX BB plume intercepts we determined BBVOC concentration using background corrected CO measured on the WP-3D.

$$BBVOC\ (ppbv) = ER_{BBVOC}(CO - CO_{bkg}) \quad \text{(E4)}$$

As shown below, BBVOC is likely the main sink of NO_3; therefore, the extent of BBVOC oxidation by NO_3 will be limited by the NO_x/BBVOC ratio as NO_x is the source for NO_3 (R1). Furthermore, the relative oxidative importance between O_3 and NO_3 depends on the NO_x/BBVOC ratio as explained by Edwards et al.[54] Therefore, in contrast to the method used for calculating BBVOC concentration in SENEX fire plume intercepts described above, we initiate our box model with fire emissions scaled to NO_x in order to preserve the NO_x/VOC ratio observed during the fire lab experiments.

To estimate the emitted NO_x at the fire source we assume that the total reactive nitrogen (NO_y, which does not include NH_3) is equivalent to the emitted NO_x. The NO_x/NO_y ratio as measured during SENEX fire plume intercepts in Figure 2 was 0.84. We calculated the observed NO_y emission ratio using NO_y (13.2 $\pm$ 3.1 ppbv) and CO (543.4 $\pm$ 87.7 ppbv) enhancements above background. The calculated NO_y emission ratio, which we assume to be the NO_x emission ratio at the fire source, was determined to be 24.3 $\pm$ 6.4 ppbv NO_y/ppmv CO for the plume intercept. We compared the estimated observed NO_x emission ratio to the NO_x emission ratios reported by Selimovic et al. for rice straw (43.9 ppbv NO_x/ppmv CO) and ponderosa pine (26.9$\pm$4.3 ppbv NO_x/ppmv CO).[23] We then scaled the BBVOC emissions by this ratio (E5), effectively scaling the fire emissions to the NO_x of the observed fire plume.

$$[BBVOC]^{model} = [BBVOC]^{inventory} * \frac{ER_{NO_y}^{observed}}{ER_{NO_x}^{inventory}} \quad \text{(E5)}$$

The NO_x emission ratio observed during the SENEX fire plume intercepts in Figure 2 was 45% and 11% lower than the laboratory-derived NO_x emission ratio for rice straw and ponderosa pine fires respectively. To correctly model the NO_3 oxidation of these fires we reduced our BBVOC emissions by a factor of 55% for rice straw and 89% for ponderosa pine.

Model background and initial concentrations of NO_x, CO, and O_3 were taken from the SENEX observations shown in Figure 2. We estimate the NO/NO_2 ratio at the fire source using the NO and NO_2 emission ratios from FIREX for each fuel. The NO/NO_2 ratios used are 5.3 and 2.8 for rice straw and ponderosa pine, respectively.[23] The background NO_2 mixing ratio was taken to be 0.9 ppbv. The background O_3 mixing ratio, 43.9 ppbv, was used as the starting O_3 mixing ratio and is representative of the background O_3 in the region where BB plumes were intercepted (Figure S3).

Box modeling was performed using the Framework for 0-D Atmospheric Modeling (F0AM)[55] to investigate the evolution of oxidized mass and oxidant fractions over 10 hours (the approximate duration of one night in July in the Southeastern U.S.). Chemical mechanisms were adopted from the MCM (v3.3.1[56–60], via website: http://mcm.york.ac.uk) and published mechanisms for methylguaiacol, syringol, *o*-guaiacol, and 3-methylfuran were added (Table S4).[61–63] Compounds not included in the above references were modeled as a one-step reaction of BBVOC + NO_3, BBVOC + O_3, or BBVOC + OH to form a single oxidation product.

All models were run at 298 K, typical experimental conditions for most published rate coefficients. Temperatures during flight ranged between 288-290 K (SI). In order to account for dilution processes, as well as entrainment of O_3, we apply a first order dilution of $k_{dil} = 1.16*10^{-5}$ s^{-1}, or a 24 hour lifetime. The sensitivity of this assumption is shown in Figure S2 and discussed in the SI. We report a base case model result with upper and lower bound uncertainties based on the emission and rate coefficient uncertainties. Although, as discussed in the SI, the bounds do not provide information on the error distribution.

Results and Discussion

In panel A of Figure 2 the power plant plume intercepts (blue background) are distinguished from the fire plume intercepts (red background) by CO, black carbon, APAN, and glyoxal. Intercepts shown in Figure 2 were at an altitude between 700-900 meters. Relative to the BB plume intercepts, the power plant plume intercepts exhibited elevated levels of NO_3 and N_2O_5 (Figure 2B). Figure 3A shows a flight map of the July 2-3 flight colored red during BB plume intercepts and sized by the APAN mixing ratio. Roughly 97% of the indicated BB plumes do not show signs of power plant plume mixing (SI). Green dashed boxes indicate sections of data shown in Figure 2.

The flight covered the intersection of Missouri, Kentucky, Tennessee, and Arkansas at the Mississippi river. According to the USDA CropScape database, this land is mainly agricultural and therefore the fire plume is most likely the result of burning crop residue and stubble.[36,64] Plume intercepts occurred near winter wheat crops, and rice straw crops are situated roughly 70 km northwest. Still, rice straw is the best available fuel proxy for agricultural burning emissions. The wind direction was roughly northwesterly with most BB plume intercepts occurring in the northwest corner of Tennessee.

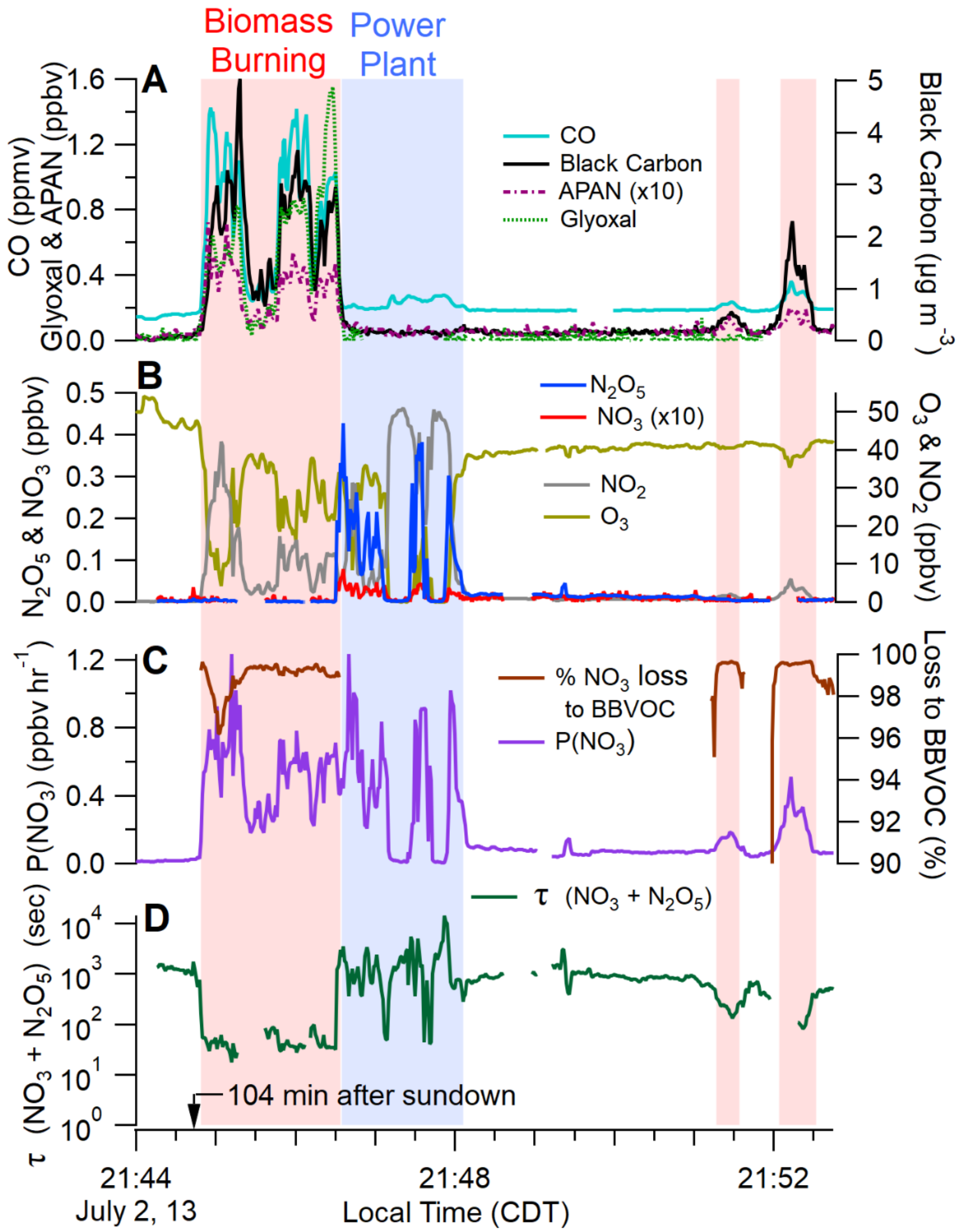

Figure 2. Time traces during representative sections of BB (red) and power plant (blue) plume intercepts made 104 minutes after sundown (SZA=90°). A: BB tracers, B: NO_3 N_2O_5, NO_2, and O_3 mixing ratio, C: production rate of NO_3 and the percentage of NO_3 reactivity toward BBVOCs, D: lifetime of NO_3 and N_2O_5.

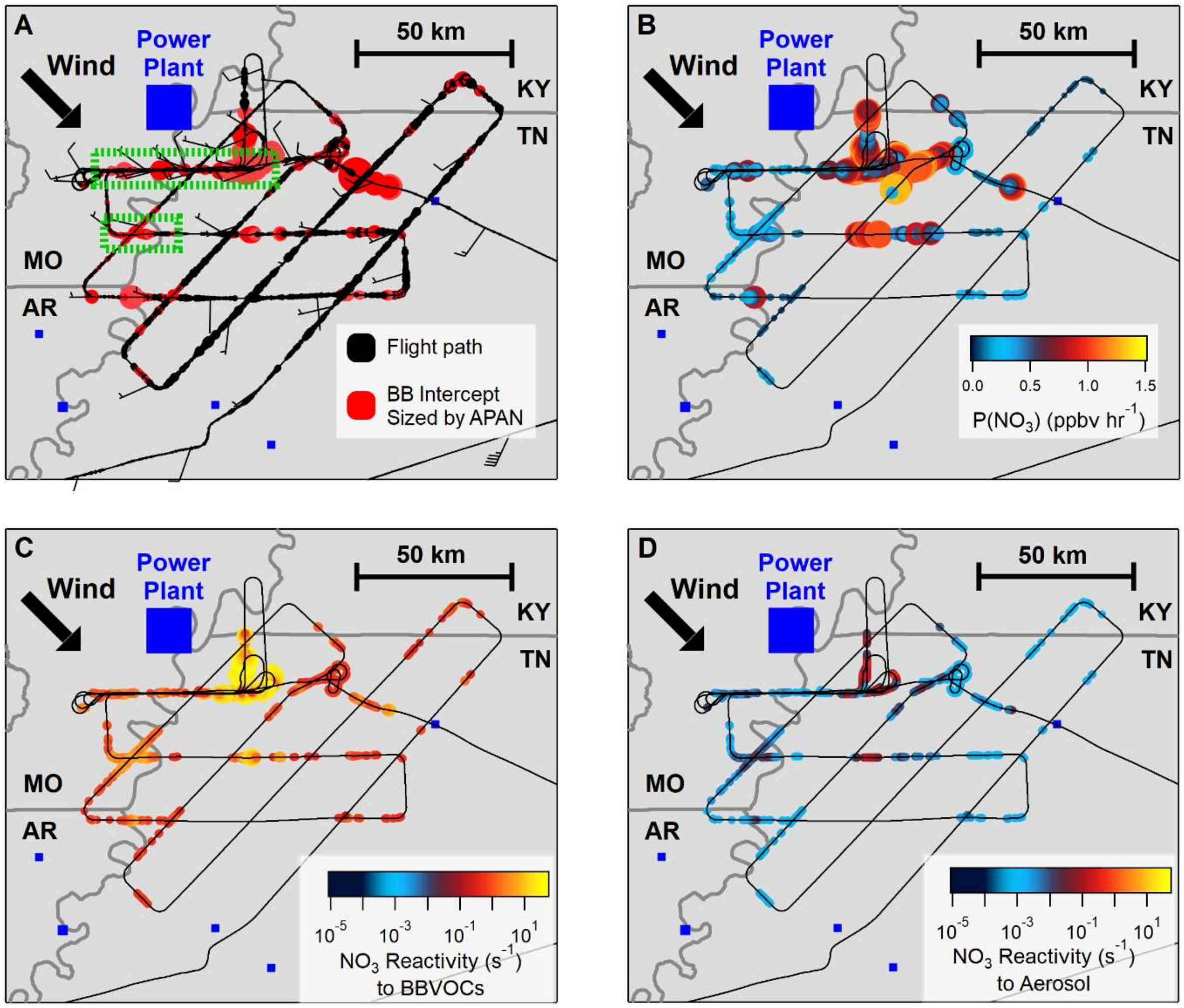

Figure 3. Flight maps of the SENEX July 2-3 2013 night flight. A: BB intercepts colored by red markers, sized by APAN (0.01-0.1 ppbv), and green dashes indicate sections shown in Figure 2, B: Production rate of NO_3, C: and D: are comparisons of NO_3 reactivity toward BBVOCs (C) and toward aerosol (D) on the same color and log scale.

To illustrate the NO_3 chemistry within a BB plume, we use previously published NO_3 and N_2O_5 analysis metrics. The NO_3 production rate, $P(NO_3)$, is the instantaneous source of NO_3 from the reaction of NO_2 with O_3 and is given in (E6).[15] The $NO_3 + N_2O_5$ lifetime (τ) is the ratio of NO_3 and N_2O_5 concentration to the NO_3 production rate (E7).[65] The summed lifetime is useful because NO_3 and N_2O_5 reach an equilibrium state that is typically more rapid than the individual sink reactions for either, such that they can be regarded as a sum.

$$P(NO_3) = k_{NO_3}[NO_2][O_3] \tag{E6}$$

$$\tau(NO_3 + N_2O_5) = \frac{NO_3 + N_2O_5}{P(NO_3)} \tag{E7}$$

$P(NO_3)$ was large and of similar magnitude in both the power plant plume and BB plume (Figure 2C). Figure 3B is colored by NO_3 production during BB intercepts only, and shows that large NO_3 production rates, near 1 ppbv hr^{-1}, were observed during multiple BB plume intercepts. Despite the large NO_3 radical production, the NO_3 and N_2O_5 concentrations within the BB plume were below the 3 pptv[38] stated detection limit of the instrument (Figure 2B), yielding short $NO_3 + N_2O_5$ lifetimes. Indeed, as shown in Figure 2D, τ is roughly a factor of 100 lower within the BB plume as compared to the power plant plume and background air. Because the NO_3 and N_2O_5 were below stated detection limits in the BB plumes, the corresponding lifetimes shown in Figure 2D are upper limits, and the actual lifetimes may be considerably shorter.

The high production rate and short lifetime of $NO_3 + N_2O_5$ within the BB plume is evidence for rapid NO_3 or N_2O_5 loss pathways. BB plumes contain large quantities of both aerosol and BBVOCs, which provide two efficient NO_3/N_2O_5 loss pathways. To understand the competition between these loss processes we calculated an instantaneous NO_3 reactivity toward aerosol and toward BBVOCs. The total NO_3 loss to BBVOC is calculated using the sum of BBVOC reactivity normalized to CO (E3). The total NO_3 loss to aerosol uptake is given as the sum of both NO_3 and N_2O_5 uptake rate coefficients. By assuming steady state[66] for both NO_3 and N_2O_5, we estimate the total aerosol uptake, and therefore NO_3 reactivity toward aerosol, as

$$k_{NO_3}^{aerosol} = K_{eq}[NO_2]k_{N_2O_5+aerosol} + k_{NO_3+aerosol} \tag{E8}$$

where $k_{NO_3}^{aerosol}$ is a first order rate coefficient, K_{eq} is the equilibrium constant between NO_3 and N_2O_5 (R2), and $k_{x+aerosol}$ is the first order rate coefficient for N_2O_5 or NO_3 aerosol uptake expressed below.

$$k_{x+aerosol} = \frac{\gamma \cdot \bar{c} \cdot SA}{4} \quad \text{(E9)}$$

Here, γ is the aerosol uptake coefficient, $\bar{c}$ is the mean molecular speed, and SA is the aerosol surface area. Calculations use uptake coefficients of $\gamma_{N_2O_5} = 10^{-2}$ for N_2O_5[19] and $\gamma_{NO_3} = 10^{-3}$ for NO_3. However, γ_{NO_3} values have a wide range therefore we include calculations with $\gamma_{NO_3} = 1$ in the SI, but find similar results.[15]

Figure 3C & D compare the NO_3 reactivity toward BBVOCs, and aerosol uptake during BB plume intercepts, respectively. In all BB intercepts, the calculated NO_3 reactivity toward BBVOCs is a factor of 100 - 1000 greater than aerosol uptake. Figure 2C shows the percentage of NO_3 reactivity dominated by BBVOC with a median >99%.

To understand which BBVOCs may be responsible for the rapid initial loss of NO_3 we calculated the relative NO_3 reactivity for 303 compounds in rice straw and ponderosa pine burning emissions. The top panel of Figure 4 shows the ranked order of the compounds that account for 99% of the rice straw initial NO_3 reactivity. Eight furan or phenol compounds are responsible for 75% of the initial NO_3 reactivity. Most of, the initial NO_3 reactivity for a rice straw fire is accounted for by phenols (60^{+20}_{-14}%) and furans (23^{+20}_{-6}%), as well as pyrroles and furfurals (8^{+9}_{-3}% combined).

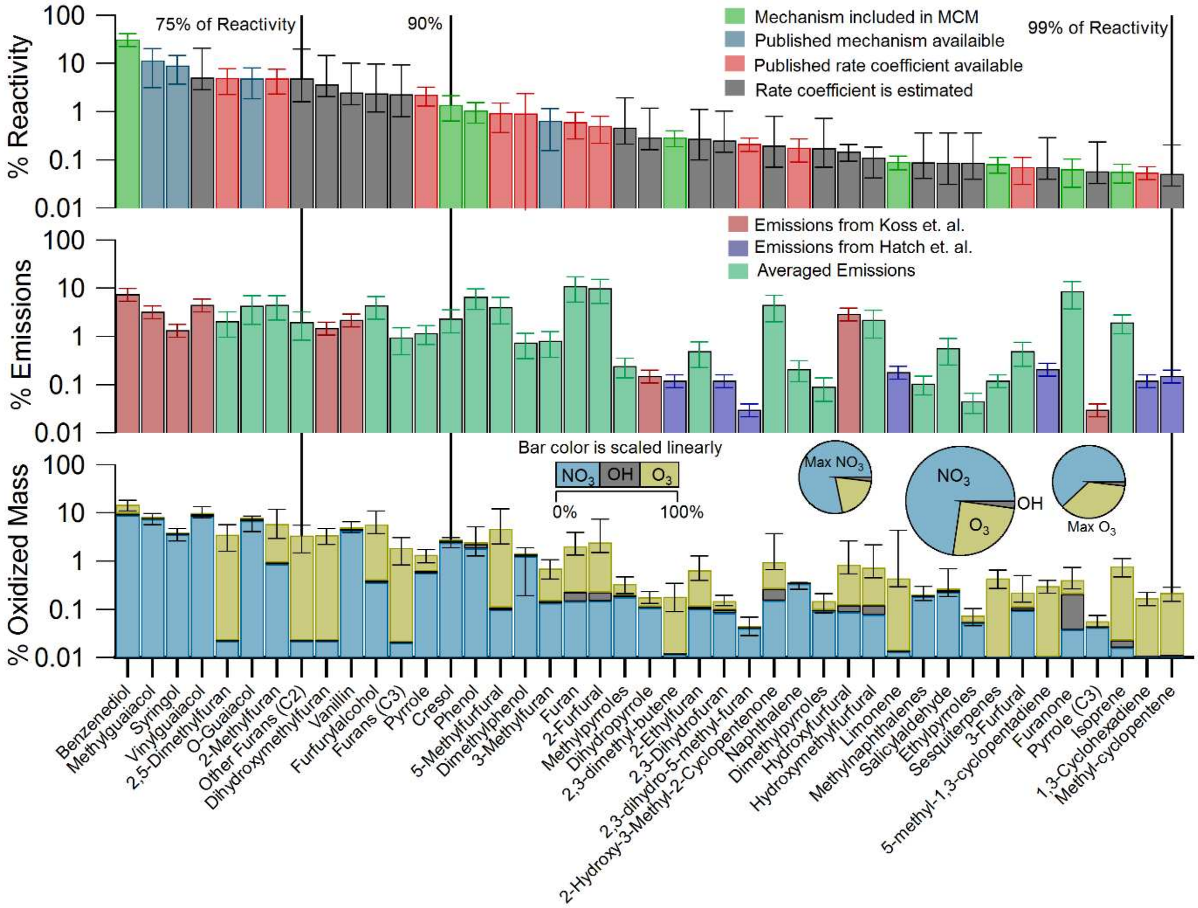

Figure 4. Rice Straw fuel. The top panel shows the ranked order of the compounds that account for 99% of the rice straw initial NO_3 reactivity. The color scale describes the origin of the mechanisms or rate coefficient used. The middle panel is the relative BBVOC emission ratio normalized to the total BBVOC emission ratio and the color scale describes the origin of the emissions data. The bottom panel is the relative nighttime reacted mass (10 hours) normalized to total reacted mass. While the bar height is on a log scale, the color scale is linear and indicates the fraction of oxidation by NO_3 (blue), O_3 (gold), and OH (grey). The center pie chart shows the fraction of reacted mass in the base case with the maximum NO_3 oxidation case to the left, and maximum O_3 oxidation case to the right. All panels sum to 100%.

The top panel of Figure 5 shows the ranked order of the compounds that account for 97% of the ponderosa pine initial NO_3 reactivity. The top 75% of initial NO_3 reactivity is distributed among 13 compounds with phenols (62^{+27}_{-23}%), furans (18^{+12}_{-4}%), pyrrole and furfural (8^{+8}_{-3}% combined) again dominating the total reactivity. Unlike rice straw, a ponderosa pine fire plume has significant reactivity towards terpenes (8^{+2}_{-1}%). The initial NO_3 reactivity towards terpenes and unsaturated hydrocarbons in a rice straw plume is <1%. These differences in reactivity are due to differences in emissions between the two fuels as explained below.[5]

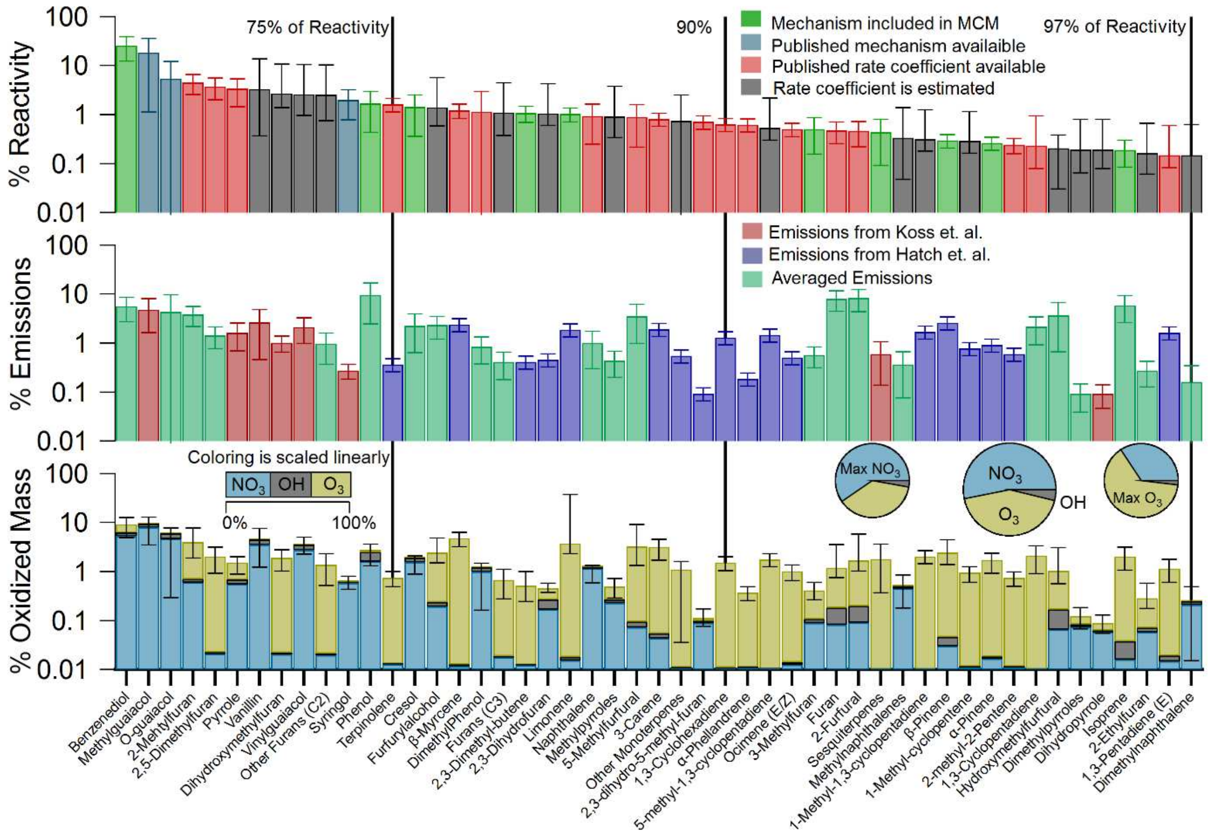

Figure 5. Same as Figure 4, but for the ponderosa pine fuel. In the bottom panel the bar height is on a log scale, but the color scale is linear and indicates the fraction of oxidation by NO_3 (blue), O_3 (gold), and OH (grey).

The middle panels of Figures 4 and 5 show the emission ratios for each compound normalized to total emissions. The color indicates the origin of the emission ratio. The rice straw fire emissions for compounds included in Figure 4 are mainly furans (33±8%), phenols (27±4%), and furfurals (24±6%), while unsaturated hydrocarbon and terpene emissions account for only 3±1%. In contrast, the ponderosa pine fire emissions have a larger representation of terpenes (18±4%) and unsaturated hydrocarbons (10±2%), but phenols (33±10%), furans (17±4%) and furfurals (18±6%) are all still significant.

To better understand smoke plume evolution and to determine the amount of BBVOC mass oxidized during one night (10 hours), we ran a 0-D box model for both rice straw and ponderosa pine fire emissions. NO_3 and N_2O_5 remained below 3 pptv (Figure S1), consistent with field observations (Figure 2B). Figure S1 illustrates that the summed concentrations of the most reactive BBVOCs are comparable to NO_2, suggesting there is approximately as much NO_3 precursor available as there is BBVOC to be oxidized. For both fuels, roughly 50-60% of NO_2 and the BBVOC compounds listed in Figure 4 and Figure 5 are depleted by chemistry (excluding dilution) in one night. Our box-model suggests several abundant BBVOCs survive the night with more than 50% of their initial starting concentration, such as phenol, furan, furfural and hydroxymethylfurfural (SI).

HNO_3 production is complex within the model, and both maximum and minimum uncertainty bounds on HNO_3 concentrations are the result of higher bound BBVOC emissions, but lower and higher bound BBVOC rate coefficients, respectively. HNO_3 is the product of reactions of phenolic compounds with NO_3, which proceeds by H-abstraction. HNO_3 production is dominated by catechol + NO_3 (~60%) within the first few hours, but as the more reactive compounds are depleted, the lesser reactive compounds like methyl guaiacol, guaiacol and syringol react with NO_3 and dominate in the last two hours. HNO_3 may be lost to the particle phase with concurrent NH_3 emission or other nitrogen species, however this loss mechanism is not included in our model.

For both fuels, catechol is the most reactive compound, and accounts for 32±9% and 26±13% of initial NO_3 reactivity at the start of the simulation for rice straw and ponderosa pine plumes, respectively. However, Koss et al.[4] were unable to distinguish between catechol and methylfurfural at m/z = 110.1 We assume a 50/50 contribution here, which yields catechol emission ratios of 2.5±0.8 ppbv ppmv^{-1} CO for rice straw and 1.5±0.6 ppbv ppmv^{-1} CO for ponderosa pine. Still, the high reactivity is mainly due to the large catechol rate coefficient ($9.9*10^{-11}$ cm^3 molecule^{-1} s^{-1})[67], which is the third greatest among the emitted compounds. Catechol is known to react with NO_3 by H-abstraction, with subsequent addition of NO_2 to the aromatic peroxy radical to form 4-nitrocatechol with a near-unity molar yield of 0.91±0.06.[68] Further, 4-nitrocatechol is expected to almost completely (96%) partition to the particle phase.[68] Recently, Hartikainen et al.[25] investigated dark oxidation of residential wood combustion and found strong correlations between the depletion of phenolic compounds and the formation of NO_3-initiated SOA. In wintertime BB events, 4-nitrocatechol and other derivatives have been detected in aerosol and are considered important light-absorbing components of brown carbon (BrC).[35,69–76]

SOA yields are a function of mass loadings.[77] Using a catechol mass loading of 300 μg m^{-3} from Finewax et al.[68] as well as a total observed aerosol plume measurement of 58.7 μg m^{-3} we estimate a 4-nitrocatechol SOA mass yield of 120%. Assuming 0.6 ppbv of catechol in ponderosa pine and 0.8 ppbv in rice straw (initial model conditions) with 44 ppbv O_3, 13 ppbv of NO_x and $k_{dil} = 1.16*10^{-5}$ s^{-1}, we estimate the SOA produced from catechol to be 3.8±1.0 μg m^{-3}

in 8 hours and $4.0^{+1.1}_{-1.0}$ μg m^{-3} in 8.5 hours for a rice straw and ponderosa pine plume, respectively. Further, there is evidence to suggest furans and furfurals may also be a source of SOA precursors.[5,25]

The bottom panel of Figure 4 shows the reacted mass per compound normalized to the total reacted mass. The bar height is on a log scale, but the bar color is linearly scaled and indicates the fraction of nighttime oxidation by NO_3 (blue), O_3 (gold), and OH (grey) after 10 hours for each compound. The center pie chart in Figure 4 and 5 represents the base case fraction of reactant mass oxidized by each oxidant. The left and right pie charts show results for the estimated maximum possible NO_3 and maximum possible O_3 oxidation, respectively. Uncertainty in the fraction of oxidized mass is calculated from the uncertainties in individual compound emissions and rate coefficients. For the compounds comprising a rice straw BB plume, the majority of mass is oxidized by NO_3 ($72^{+6}_{-11}\%$). This is expected because the rice straw fuel emissions are rich in oxygenated aromatic and hetero-aromatic emissions, which are generally less reactive toward O_3. Terpenes and unsaturated hydrocarbons, which are a small fraction of emissions in Figure 4, are relatively more reactive toward O_3. Even so, O_3 still has a significant oxidative impact and is responsible for $26^{+11}_{-6}\%$ of oxidized BBVOC mass.

The relative amount of oxidized mass for ponderosa pine is shown in the bottom panel of Figure 5. Almost half of the oxidized mass for compounds included in Figure 5 is due to O_3 ($43^{+21}_{-6}\%$) for our base case. The phenolic compounds mainly undergo NO_3 oxidation while terpenes and unsaturated hydrocarbons are mainly oxidized by O_3. Furans and the hetero-aromatics are oxidized approximately evenly by O_3 and NO_3. The increased fraction of O_3 oxidation is the result of the increased fraction of unsaturated hydrocarbon and terpenes in the ponderosa pine emissions when compared to rice straw.

The nighttime chemical evolution and oxidation products of a biomass burning plume will depend on the relative NO_3 and O_3 reactivity. Neglecting the small contribution from OH oxidation, Edwards et al.[54] show the competition between NO_3 and O_3 oxidation of biogenic VOCs (BVOC) is dependent on the NO_x/BVOC ratio. We scaled our BBVOC emissions to maintain the NO_x/BBVOC ratio expected for rice straw (0.4 ± 0.1) or ponderosa pine (0.3 ± 0.1) emissions. However, because fires are highly variable, the NO_x/BBVOC ratio for any given fuel may vary from fire to fire. For rice straw, a factor of two increase in NO_x increases the fraction of NO_3 oxidation from 72% to 84%, while a factor of two decrease in NO_x decreases relative NO_3 oxidation to 55%. Similarly, for ponderosa pine, doubling NO_x increases the fraction of NO_3 oxidation from 53% to 66%, while halving NO_x decreases relative NO_3 oxidation to 37% and increases O_3 to 57%. Furthermore, we find that a factor of two change in ambient O_3 concentration has little effect on the relative NO_3 and O_3 reactivity (see SI).

Our reactivity calculations and box-model results are most limited by a lack of kinetic and mechanistic studies for O_3, NO_3, and OH + BBVOCs reactions. Kinetic and mechanistic studies of furan, furfural, phenol, and pyrrole analogues reacting with NO_3 will be most critical to understanding nighttime BB processes, which we highlight in the SI.

The time of day in which a fire is active will determine the fate of its emissions. This paper presents the first nighttime aircraft intercepts of a BB plume combined with an inventory of 303 BBVOC emissions and an oxidation model to predict the lifetime and fate of BB emissions in the dark. Fire emissions at times near sunset will undergo the chemistry we have detailed here, which suggests a roughly 60% depletion (for both rice straw and ponderosa pine) of fire-derived NO_x. We find that nighttime chemistry is likely to proceed by NO_3, rather than N_2O_5, further slowing the loss of NO_x (R1 & R2). Our model applies to chemistry at the center of a plume and does not include dispersion. Dispersion mixes NO_x with background O_3 at the edges of the plume leading to faster depletion, and therefore the values we report are likely lower limits. Even so, 18-19% of BBVOC mass, out of the total BBVOC mass that we model, will be oxidized in one night. That is roughly a 55% depletion of the BBVOCs that are reactive toward NO_3. There is evidence that many of these NO_3 reactive compounds can form secondary BrC aerosol[35,69–76], suggesting nighttime oxidation may be a significant source of BB derived BrC. Furthermore, future BB photochemical models should consider that these reactive phenolic-, furan- and furfural-like compounds are not only reactive toward NO_3, but also O_3 and OH, thus affecting next-day BB photochemistry.

Acknowledgments

We'd like to thank Charles A. Brock for aerosol surface area measurements.

Supporting Information Available

Figure S1, box model time traces of key species, Figure S2, box model sensitivity to the dilution rate coefficient, Figure S3, Correlation of O_3 and NO_2 from aircraft observations, Figure S4, altitude profiles of key species and potential temperature, Figure S5, plume age estimates, Figure S6, variability in emission ratios. Table S1, BB plume and background values, Table S2, Plumes and background times, Table S3, List of reactions excluded from the MCM, Table S4, mechanisms added to the MCM. This information is available free of charge via the Internet at http://pubs.acs.org.

References

(1) Dennison, P. E.; Brewer, S. C.; Arnold, J. D.; Moritz, M. A. Large Wildfire Trends in the Western United States, 1984-2011. *Geophys. Res. Lett.* **2014**, *41*, 2014GL059576.

https://doi.org/10.1002/2014gl059576.

(2) Westerling, A. L.; Hidalgo, H. G.; Cayan, D. R.; Swetnam, T. W. Warming and Earlier Spring Increase Western U.S. Forest Wildfire Activity. *Science (80-.).* **2006**, *313* (5789), 940–943.

(3) Pope, C. A.; Dockery, D. W. Health Effects of Fine Particulate Air Pollution: Lines That Connect. *J. Air Waste Manag. Assoc.* **2006**, *56* (6), 709–742. https://doi.org/10.1080/10473289.2006.10464485.

(4) Koss, A. R.; Sekimoto, K.; Gilman, J. B.; Selimovic, V.; Coggon, M. M.; Zarzana, K. J.; Yuan, B.; Lerner, B. M.; Brown, S. S.; Jimenez, J. L.; Krechmer, J.; Roberts, J. M.; Warneke, C.; Yokelson, R. J.; de Gouw, J. Non-Methane Organic Gas Emissions from Biomass Burning: Identification, Quantification, and Emission Factors from PTR-ToF during the FIREX 2016 Laboratory Experiment. *Atmos. Chem. Phys.* **2018**, *18* (October), 3299–3319. https://doi.org/10.5194/acp-2017-924.

(5) Hatch, L. E.; Yokelson, R. J.; Stockwell, C. E.; Veres, P. R.; Simpson, I. J.; Blake, D. R.; Orlando, J. J.; Barsanti, K. C. Multi-Instrument Comparison and Compilation of Non-Methane Organic Gas Emissions from Biomass Burning and Implications for Smoke-Derived Secondary Organic Aerosol Precursors. *Atmos. Chem. Phys.* **2017**, *17* (2), 1471–1489. https://doi.org/10.5194/acp-17-1471-2017.

(6) Rotstayn, L. D.; Penner, J. E. Indirect Aerosol Forcing, Quasi Forcing, and Climate Response. *J. Clim.* **2001**, *14* (13), 2960–2975. https://doi.org/10.1175/1520-0442(2001)014<2960:IAFQFA>2.0.CO;2.

(7) Andreae, M. O.; Merlet, P. Emission of Trace Gases and Aerosols from Biomass Burning.

Global Biogeochem. Cycles **2001**, *15* (4), 955–966. https://doi.org/10.1029/2000GB001382.

(8) Yokelson, R. J.; Crounse, J. D.; DeCarlo, P. F.; Karl, T.; Urbanski, S.; Atlas, E.; Campos, T.; Shinozuka, Y.; Kapustin, V.; Clarke, A. D.; Weinheimer, A.; Knapp, D. J.; Montzka, D. D.; Holloway, J.; Weibring, P.; Flocke, F.; Zheng, W.; Toohey, D.; Wennberg, P. O.; Wiedinmyer, C.; Mauldin, L.; Fried, A.; Richter, D.; Walega, J.; Jimenez, J. L.; Adachi, K.; Buseck, P. R.; Hall, S. R.; Shetter, R. Emissions from Biomass Burning in the Yucatan. *Atmos. Chem. Phys.* **2009**, *9* (15), 5785–5812. https://doi.org/10.5194/acp-9-5785-2009.

(9) Hennigan, C. J.; Sullivan, A. P.; Collett, J. L.; Robinson, A. L. Levoglucosan Stability in Biomass Burning Particles Exposed to Hydroxyl Radicals. *Geophys. Res. Lett.* **2010**, *37* (9), 1–4. https://doi.org/10.1029/2010GL043088.

(10) Hennigan, C. J.; Miracolo, M. A.; Engelhart, G. J.; May, A. A.; Presto, A. A.; Lee, T.; Sullivan, A. P.; McMeeking, G. R.; Coe, H.; Wold, C. E.; Hao, W. M.; Gilman, J. B.; Kuster, W. C.; De Gouw, J.; Schichtel, B. A.; Collett, J. L.; Kreidenweis, S. M.; Robinson, A. L. Chemical and Physical Transformations of Organic Aerosol from the Photo-Oxidation of Open Biomass Burning Emissions in an Environmental Chamber. *Atmos. Chem. Phys.* **2011**, *11* (15), 7669–7686. https://doi.org/10.5194/acp-11-7669-2011.

(11) Ortega, A. M.; Day, D. A.; Cubison, M. J.; Brune, W. H.; Bon, D.; De Gouw, J. A.; Jimenez, J. L. Secondary Organic Aerosol Formation and Primary Organic Aerosol Oxidation from Biomass-Burning Smoke in a Flow Reactor during FLAME-3. *Atmos. Chem. Phys.* **2013**, *13* (22), 11551–11571. https://doi.org/10.5194/acp-13-11551-2013.

(12) Bruns, E. A.; El Haddad, I.; Slowik, J. G.; Kilic, D.; Klein, F.; Baltensperger, U.; Prévôt, A. S. H. Identification of Significant Precursor Gases of Secondary Organic Aerosols from Residential Wood Combustion. *Sci. Rep.* **2016**, *6* (June), 1–9. https://doi.org/10.1038/srep27881.

(13) Bruns, E. A.; El Haddad, I.; Keller, A.; Klein, F.; Kumar, N. K.; Pieber, S. M.; Corbin, J. C.; Slowik, J. G.; Brune, W. H.; Baltensperger, U.; Prévôt, A. S. H. Inter-Comparison of Laboratory Smog Chamber and Flow Reactor Systems on Organic Aerosol Yield and Composition. *Atmos. Meas. Tech.* **2015**, *8* (6), 2315–2332. https://doi.org/10.5194/amt-8-2315-2015.

(14) Jaffe, D. A.; Wigder, N. L. Ozone Production from Wildfires: A Critical Review. *Atmos. Environ.* **2012**, *51*, 1–10. https://doi.org/http://dx.doi.org/10.1016/j.atmosenv.2011.11.063.

(15) Brown, S. S.; Stutz, J. Nighttime Radical Observations and Chemistry. *Chem. Soc. Rev.* **2012**, *41*, 6405–6447. https://doi.org/10.1039/c2cs35181a.

(16) Wayne, R. .; Barnes, I.; Biggs, P.; Burrows, J. .; Canosa-Mas, C. .; Hjorth, J.; Le Bras, G.; Moortgat, G. .; Perner, D.; Poulet, G.; Restelli, G.; Sidebottom, H. The Nitrate Radical: Physics, Chemistry, and the Atmosphere. *Atmos. Environ. Part A. Gen. Top.* **1991**, *25* (1), 1–203. https://doi.org/10.1016/0960-1686(91)90192-A.

(17) Osthoff, H. D.; Roberts, J. M.; Ravishankara, A. R.; Williams, E. J.; Lerner, B. M.; Sommariva, R.; Bates, T. S.; Coffman, D.; Quinn, P. K.; Dibb, J. E.; Stark, H.; Burkholder, J. B.; Talukdar, R. K.; Meagher, J.; Fehsenfeld, F. C.; Brown, S. S. High Levels of Nitryl Chloride in the Polluted Subtropical Marine Boundary Layer. *Nat. Geosci.* **2008**, *1* (5), 324–328. https://doi.org/10.1038/ngeo177.

(18) Thornton, J. A.; Kercher, J. P.; Riedel, T. P.; Wagner, N. L.; Cozic, J.; Holloway, J. S.; Dubé, W. P.; Wolfe, G. M.; Quinn, P. K.; Middlebrook, A. M.; Alexander, B.; Brown, S. S. A Large Atomic Chlorine Source Inferred from Mid-Continental Reactive Nitrogen Chemistry. *Nature* **2010**, *464* (7286), 271–274. https://doi.org/10.1038/nature08905.

(19) Chang, W. L.; Bhave, P. V.; Brown, S. S.; Riemer, N.; Stutz, J.; Dabdub, D. Heterogeneous Atmospheric Chemistry, Ambient Measurements, and Model Calculations of N2O5: A Review. *Aerosol Sci. Technol.* **2011**, *45* (6), 655–685. https://doi.org/10.1080/02786826.2010.551672.

(20) Ahern, A.; Goldberger, L.; Jahl, L.; Thornton, J.; Sullivan, R. C. Production of N2O5 and ClNO2 through Nocturnal Processing of Biomass-Burning Aerosol. *Environ. Sci. Technol.* **2018**, *52* (2), 550–559. https://doi.org/10.1021/acs.est.7b04386.

(21) Hatch, L. E.; Luo, W.; Pankow, J. F.; Yokelson, R. J.; Stockwell, C. E.; Barsanti, K. C. Identification and Quantification of Gaseous Organic Compounds Emitted from Biomass Burning Using Two-Dimensional Gas Chromatography–time-of-Flight Mass Spectrometry. *Atmos. Chem. Phys.* **2015**, *15* (4), 1865–1899. https://doi.org/10.5194/acp-15-1865-2015.

(22) Stockwell, C. E.; Yokelson, R. J.; Kreidenweis, S. M.; Robinson, A. L.; Demott, P. J.; Sullivan, R. C.; Reardon, J.; Ryan, K. C.; Griffith, D. W. T.; Stevens, L. Trace Gas Emissions from Combustion of Peat, Crop Residue, Domestic Biofuels, Grasses, and Other Fuels: Configuration and Fourier Transform Infrared (FTIR) Component of the Fourth Fire Lab at Missoula Experiment (FLAME-4). *Atmos. Chem. Phys.* **2014**, *14* (18), 9727–9754. https://doi.org/10.5194/acp-14-9727-2014.

(23) Selimovic, V.; Yokelson, R. J.; Warneke, C.; Roberts, J. M.; de Gouw, J. A.; Griffith, D. W. T. Aerosol Optical Properties and Trace Gas Emissions from Laboratory-Simulated Western US Wildfires during FIREX. *Atmos. Chem. Phys.* **2017**, *18*, 2929–2948. https://doi.org/10.5194/acp-18-2929-2018.

(24) Sekimoto, K.; Koss, A. R.; Gilman, J. B.; Selimovic, V.; Coggon, M. M.; Zarzana, K. J.; Yuan, B.; Lerner, B. M.; Brown, S. S.; Warneke, C.; Yokelson, R. J.; Roberts, J. M.; de Gouw, J. High- and Low-Temperature Pyrolysis Profiles Describe Volatile Organic Compound Emissions from Western US Wildfire Fuels. *Atmos. Chem. Phys. Discuss.* **2018**, No. February, 1–39. https://doi.org/10.5194/acp-2018-52.

(25) Hartikainen, A.; Yli-Pirilä, P.; Tiitta, P.; Leskinen, A.; Kortelainen, M.; Orasche, J.; Schnelle-Kreis, J.; Lehtinen, K.; Zimmermann, R.; Jokiniemi, J.; Sippula, O. Volatile Organic Compounds from Logwood Combustion: Emissions and Transformation under Dark and Photochemical Aging Conditions in a Smog Chamber. *Environ. Sci. Technol.* **2018**, *52* (4979–4988), acs.est.7b06269. https://doi.org/10.1021/acs.est.7b06269.

(26) Atkinson, R.; Arey, J. Gas-Phase Tropospheric Chemistry of Biogenic Volatile Organic Compounds: A Review. In *Atmospheric Environment*; Pergamon, 2003; Vol. 37, pp 197–219. https://doi.org/10.1016/S1352-2310(03)00391-1.

(27) Atkinson, R.; Arey, J. Atmospheric Degradation of Volatile Organic Compounds. *Chem. Rev.* **2003**, *103* (3), 4605–4638. https://doi.org/10.1021/cr0206420.

(28) Atkinson, R. Kinetics and Mechanisms of the Gas-Phase Reactions of the NO3 Radical with Organic Compounds. *Journal of Physical and Chemical Reference Data*. 1991, pp 459–507. https://doi.org/10.1063/1.555887.

(29) El Zein, A.; Coeur, C.; Obeid, E.; Lauraguais, A.; Fagniez, T. Reaction Kinetics of Catechol (1,2-Benzenediol) and Guaiacol (2-Methoxyphenol) with Ozone. *J. Phys. Chem. A* **2015**, *119* (26), 6759–6765. https://doi.org/10.1021/acs.jpca.5b00174.

(30) Martínez, E.; Cabañas, B.; Aranda, A.; Martín, P.; Salgado, S. Absolute Rate Coefficients for the Gas-Phase Reactions of NO3 Radical with a Series of Monoterpenes at T = 298 to 433 K. *J. Atmos. Chem.* **1999**, *33* (3), 265–282. https://doi.org/10.1023/A:1006178530211.

(31) Kerdouci, J.; Picquet-Varrault, B.; Doussin, J. F. Structure-Activity Relationship for the Gas-Phase Reactions of NO3radical with Organic Compounds: Update and Extension to Aldehydes. *Atmos. Environ.* **2014**, *84* (3), 363–372. https://doi.org/10.1016/j.atmosenv.2013.11.024.

(32) Grosjean, D.; Williams, E. L. Environmental Persistence of Organic Compounds Estimated from Structure-Reactivity and Linear Free-Energy Relationships. Unsaturated Aliphatics. *Atmos. Environ. Part A, Gen. Top.* **1992**, *26* (8), 1395–1405. https://doi.org/10.1016/0960-1686(92)90124-4.

(33) Cabañas, B.; Baeza, M. T.; Salgado, S.; Martín, P.; Taccone, R.; Martínez, E. Oxidation of Heterocycles in the Atmosphere: Kinetic Study of Their Reactions with NO3 Radical. *J. Phys. Chem. A* **2004**, *108* (49), 10818–10823. https://doi.org/10.1021/jp046524t.

(34) Harrison, M. A. J.; Barra, S.; Borghesi, D.; Vione, D.; Arsene, C.; Iulian Olariu, R. Nitrated Phenols in the Atmosphere: A Review. *Atmospheric Environment*. 2005, pp 231–248. https://doi.org/10.1016/j.atmosenv.2004.09.044.

(35) Laskin, A.; Laskin, J.; Nizkorodov, S. A. Chemistry of Atmospheric Brown Carbon.

Chem. Rev. **2015**, *115* (10), 4335–4382. https://doi.org/10.1021/cr5006167.

(36) Zarzana, K. J.; Min, K. E.; Washenfelder, R. A.; Kaiser, J.; Krawiec-Thayer, M.; Peischl, J.; Neuman, J. A.; Nowak, J. B.; Wagner, N. L.; Dubè, W. P.; Clair, J. M. S.; Wolfe, G. M.; Hanisco, T. F.; Keutsch, F. N.; Ryerson, T. B.; Brown, S. S. Emissions of Glyoxal and Other Carbonyl Compounds from Agricultural Biomass Burning Plumes Sampled by Aircraft. *Environ. Sci. Technol.* **2017**, *51* (20), 11761–11770. https://doi.org/10.1021/acs.est.7b03517.

(37) Neuman, J. A.; Trainer, M.; Brown, S. S.; Min, K. E.; Nowak, J. B.; Parrish, D. D.; Peischl, J.; Pollack, I. B.; Roberts, J. M.; Ryerson, T. B.; Veres, P. R. HONO Emission and Production Determined from Airborne Measurements over the Southeast U.S. *J. Geophys. Res.* **2016**, *121* (15), 9237–9250. https://doi.org/10.1002/2016JD025197.

(38) Warneke, C.; Trainer, M.; De Gouw, J. A.; Parrish, D. D.; Fahey, D. W.; Ravishankara, A. R.; Middlebrook, A. M.; Brock, C. A.; Roberts, J. M.; Brown, S. S.; Neuman, J. A.; Lerner, B. M.; Lack, D.; Law, D.; Hübler, G.; Pollack, I.; Sjostedt, S.; Ryerson, T. B.; Gilman, J. B.; Liao, J.; Holloway, J.; Peischl, J.; Nowak, J. B.; Aikin, K. C.; Min, K. E.; Washenfelder, R. A.; Graus, M. G.; Richardson, M.; Markovic, M. Z.; Wagner, N. L.; Welti, A.; Veres, P. R.; Edwards, P.; Schwarz, J. P.; Gordon, T.; Dube, W. P.; McKeen, S. A.; Brioude, J.; Ahmadov, R.; Bougiatioti, A.; Lin, J. J.; Nenes, A.; Wolfe, G. M.; Hanisco, T. F.; Lee, B. H.; Lopez-Hilfiker, F. D.; Thornton, J. A.; Keutsch, F. N.; Kaiser, J.; Mao, J.; Hatch, C. D. Instrumentation and Measurement Strategy for the NOAA SENEX Aircraft Campaign as Part of the Southeast Atmosphere Study 2013. *Atmos. Meas. Tech.* **2016**, *9* (7), 3063–3093. https://doi.org/10.5194/amt-9-3063-2016.

(39) Brown, S. S.; Stark, H.; Ravishankara, A. R. Cavity Ring-down Spectroscopy for Atmospheric Trace Gas Detection: Application to the Nitrate Radical (NO3). *Appl. Phys. B Lasers Opt.* **2002**, *75* (2–3), 173–182. https://doi.org/10.1007/s00340-002-0980-y.

(40) Dubé, W. P.; Brown, S. S.; Osthoff, H. D.; Nunley, M. R.; Ciciora, S. J.; Paris, M. W.; McLaughlin, R. J.; Ravishankara, A. R. Aircraft Instrument for Simultaneous, *in Situ* Measurement of NO3 and N2O5 via Pulsed Cavity Ring-down Spectroscopy. *Rev. Sci. Instrum.* **2006**, *77* (3), 034101. https://doi.org/10.1063/1.2176058.

(41) Fuchs, H.; Dubé, W. P.; Ciciora, S. J.; Brown, S. S. Determination of Inlet Transmission and Conversion Efficiencies for in Situ Measurements of the Nocturnal Nitrogen Oxides, NO3, N 2O5 and NO2, via Pulsed Cavity Ring-down Spectroscopy. *Anal. Chem.* **2008**, *80* (15), 6010–6017. https://doi.org/10.1021/ac8007253.

(42) Wild, R. J.; Edwards, P. M.; Dube, W. P.; Baumann, K.; Edgerton, E. S.; Quinn, P. K.; Roberts, J. M.; Rollins, A. W.; Veres, P. R.; Warneke, C.; Williams, E. J.; Yuan, B.; Brown, S. S.; Dubé, W. P.; Baumann, K.; Edgerton, E. S.; Quinn, P. K.; Roberts, J. M.; Rollins, A. W.; Veres, P. R.; Warneke, C.; Williams, E. J.; Yuan, B.; Brown, S. S. A Measurement of Total Reactive Nitrogen, NOy, Together with NO2, NO, and O3 via Cavity Ring-down Spectroscopy. *Environ. Sci. Technol.* **2014**, *48* (16), 9609–9615. https://doi.org/10.1021/es501896w.

(43) Ryerson, T. B.; Huey, L. G.; Knapp, K.; Nueman, J. A.; Parrish, D. D.; Sueper, D. T.; Fehsenfeld, F. C. Design and Initial Characterization of an Inlet for Gas-Phase NOy Measurements from Aircraf. *J. Geophys. Res. Atmos.* **1999**, *104* (D5), 5483–5492.

(44) Brock, C. A.; Schröder, F.; Kärcher, B.; Petzold, A.; Busen, R.; Fiebig, M. Ultrafine

Particle Size Distribution Measured in Aircraft Exhaust Plumes. *J. Geophys. Res.* **2000**, *105* (Vi), 26555–26567.

(45) Brock, C. A.; Cozic, J.; Bahreini, R.; Froyd, K. D.; Middlebrook, A. M.; McComiskey, A.; Brioude, J.; Cooper, O. R.; Stohl, A.; Aikin, K. C.; De Gouw, J. A.; Fahey, D. W.; Ferrare, R. A.; Gao, R. S.; Gore, W.; Holloway, J. S.; Hübler, G.; Jefferson, A.; Lack, D. A.; Lance, S.; Moore, R. H.; Murphy, D. M.; Nenes, A.; Novelli, P. C.; Nowak, J. B.; Ogren, J. A.; Peischl, J.; Pierce, R. B.; Pilewskie, P.; Quinn, P. K.; Ryerson, T. B.; Schmidt, K. S.; Schwarz, J. P.; Sodemann, H.; Spackman, J. R.; Stark, H.; Thomson, D. S.; Thornberry, T.; Veres, P.; Watts, L. A.; Warneke, C.; Wollny, A. G. Characteristics, Sources, and Transport of Aerosols Measured in Spring 2008 during the Aerosol, Radiation, and Cloud Processes Affecting Arctic Climate (ARCPAC) Project. *Atmos. Chem. Phys.* **2011**, *11* (6), 2423–2453. https://doi.org/10.5194/acp-11-2423-2011.

(46) De Gouw, J.; Warneke, C. Measurements of Volatile Organic Compounds in the Earth's Atmosphere Using Proton-Transfer-Reaction Mass Spectrometry. *Mass Spectrometry Reviews*. Wiley-Blackwell March 1, 2007, pp 223–257. https://doi.org/10.1002/mas.20119.

(47) Bond, T. C.; Doherty, S. J.; Fahey, D. W.; Forster, P. M.; Berntsen, T.; Deangelo, B. J.; Flanner, M. G.; Ghan, S.; Kärcher, B.; Koch, D.; Kinne, S.; Kondo, Y.; Quinn, P. K.; Sarofim, M. C.; Schultz, M. G.; Schulz, M.; Venkataraman, C.; Zhang, H.; Zhang, S.; Bellouin, N.; Guttikunda, S. K.; Hopke, P. K.; Jacobson, M. Z.; Kaiser, J. W.; Klimont, Z.; Lohmann, U.; Schwarz, J. P.; Shindell, D.; Storelvmo, T.; Warren, S. G.; Zender, C. S. Bounding the Role of Black Carbon in the Climate System: A Scientific Assessment. *J. Geophys. Res. Atmos.* **2013**, *118* (11), 5380–5552. https://doi.org/10.1002/jgrd.50171.

(48) Min, K.-E.; Washenfelder, R. a.; Dubé, W. P.; Langford, a. O.; Edwards, P. M.; Zarzana, K. J.; Stutz, J.; Lu, K.; Rohrer, F.; Zhang, Y.; Brown, S. S. A Broadband Cavity Enhanced Absorption Spectrometer for Aircraft Measurements of Glyoxal, Methylglyoxal, Nitrous Acid, Nitrogen Dioxide, and Water Vapor. *Atmos. Meas. Tech. Discuss.* **2016**, *9* (10), 423–440. https://doi.org/10.5194/amtd-8-11209-2015.

(49) Zheng, W.; Flocke, F. M.; Tyndall, G. S.; Swanson, A.; Orlando, J. J.; Roberts, J. M.; Huey, L. G.; Tanner, D. J. Characterization of a Thermal Decomposition Chemical Ionization Mass Spectrometer for the Measurement of Peroxy Acyl Nitrates (PANs) in the Atmosphere. *Atmos. Chem. Phys.* **2011**, *11* (13), 6529–6547. https://doi.org/10.5194/acp-11-6529-2011.

(50) Schwarz, J. P.; Gao, R. S.; Fahey, D. W.; Thomson, D. S.; Watts, L. A.; Wilson, J. C.; Reeves, J. M.; Darbeheshti, M.; Baumgardner, D. G.; Kok, G. L.; Chung, S. H.; Schulz, M.; Hendricks, J.; Lauer, A.; Kärcher, B.; Slowik, J. G.; Rosenlof, K. H.; Thompson, T. L.; Langford, A. O.; Loewenstein, M.; Aikin, K. C. Single-Particle Measurements of Midlatitude Black Carbon and Light-Scattering Aerosols from the Boundary Layer to the Lower Stratosphere. *J. Geophys. Res. Atmos.* **2006**, *111* (16), 1–15. https://doi.org/10.1029/2006JD007076.

(51) Holloway, J. S.; Jakoubek, R. O.; Parrish, D. D.; Gerbig, C.; Volz-Thomas, A.; Schmitgen, S.; Fried, A.; Wert, B.; Henry, B.; Drummond, J. R. Airborne Intercomparison of Vacuum Ultraviolet Fluorescence and Tunable Diode Laser Absorption Measurements of Tropospheric Carbon Monoxide. *J. Geophys. Res. Atmos.* **2000**, *105* (D19), 24251–24261. https://doi.org/10.1029/2000JD900237.

(52) Stockwell, C. E.; Veres, P. R.; Williams, J.; Yokelson, R. J. Characterization of Biomass Burning Emissions from Cooking Fires, Peat, Crop Residue, and Other Fuels with High-Resolution Proton-Transfer-Reaction Time-of-Flight Mass Spectrometry. *Atmos. Chem. Phys.* **2015**, *15* (2), 845–865. https://doi.org/10.5194/acp-15-845-2015.

(53) Kerdouci, J.; Picquet-Varrault, B.; Doussin, J. F. Prediction of Rate Constants for Gas-Phase Reactions of Nitrate Radical with Organic Compounds: A New Structure-Activity Relationship. *ChemPhysChem* **2010**, *11* (18), 3909–3920. https://doi.org/10.1002/cphc.201000673.

(54) Edwards, P. M.; Aikin, K. C.; Dube, W. P.; Fry, J. L.; Gilman, J. B.; De Gouw, J. A.; Graus, M. G.; Hanisco, T. F.; Holloway, J.; Hübler, G.; Kaiser, J.; Keutsch, F. N.; Lerner, B. M.; Neuman, J. A.; Parrish, D. D.; Peischl, J.; Pollack, I. B.; Ravishankara, A. R.; Roberts, J. M.; Ryerson, T. B.; Trainer, M.; Veres, P. R.; Wolfe, G. M.; Warneke, C. Transition from High- to Low-NO x Control of Night-Time Oxidation in the Southeastern US. *Nat. Geosci.* **2017**, *10* (7), 490–495. https://doi.org/10.1038/ngeo2976.

(55) Wolfe, G. M.; Marvin, M. R.; Roberts, S. J.; Travis, K. R.; Liao, J. The Framework for 0-D Atmospheric Modeling (F0AM) v3.1. *Geosci. Model Dev.* **2016**, *9* (9), 3309–3319. https://doi.org/10.5194/gmd-9-3309-2016.

(56) Jenkin, M. E.; Saunders, S. M.; Pilling, M. J. The Tropospheric Degradation of Volatile Organic Compounds: A Protocol for Mechanism Development. *Atmos. Environ.* **1997**, *31* (1), 81–104. https://doi.org/10.1016/S1352-2310(96)00105-7.

(57) Jenkin, M. E.; Saunders, S. M.; Wagner, V.; Pilling, M. J. Protocol for the Development of the Master Chemical Mechanism, MCM v3 (Part B): Tropospheric Degradation of

Aromatic Volatile Organic Compounds. *Atmos. Chem. Phys.* **2003**, *3* (1), 181–193. https://doi.org/10.5194/acp-3-181-2003.

(58) Bloss, C.; Wagner, V.; Jenkin, M. E.; Volkamer, R.; Bloss, W. J.; Lee, J. D.; Heard, D. E.; Wirtz, K.; Martin-Reviejo, M.; Rea, G.; Wenger, J. C.; Pilling, M. J. Development of a Detailed Chemical Mechanism (MCMv3.1) for the Atmospheric Oxidation of Aromatic Hydrocarbons. *Atmos. Chem. Phys.* **2005**, *5* (3), 641–664. https://doi.org/10.5194/acp-5-641-2005.

(59) Jenkin, M. E.; Wyche, K. P.; Evans, C. J.; Carr, T.; Monks, P. S.; Alfarra, M. R.; Barley, M. H.; McFiggans, G. B.; Young, J. C.; Rickard, A. R. Development and Chamber Evaluation of the MCM v3.2 Degradation Scheme for β-Caryophyllene. *Atmos. Chem. Phys.* **2012**, *12* (11), 5275–5308. https://doi.org/10.5194/acp-12-5275-2012.

(60) Jenkin, M. E.; Young, J. C.; Rickard, A. R. The MCM v3.3.1 Degradation Scheme for Isoprene. *Atmos. Chem. Phys.* **2015**, *15* (20), 11433–11459. https://doi.org/10.5194/acp-15-11433-2015.

(61) Yang, B.; Zhang, H.; Wang, Y.; Zhang, P.; Shu, J.; Sun, W.; Ma, P. Experimental and Theoretical Studies on Gas-Phase Reactions of NO3 Radicals with Three Methoxyphenols: Guaiacol, Creosol, and Syringol. *Atmos. Environ.* **2016**, *125* (3), 243–251. https://doi.org/10.1016/j.atmosenv.2015.11.028.

(62) Tapia, A.; Villanueva, F.; Salgado, M. S.; Cabañas, B.; Martínez, E.; Martín, P. Atmospheric Degradation of 3-Methylfuran: Kinetic and Products Study. *Atmos. Chem. Phys.* **2011**, *11* (7), 3227–3241. https://doi.org/10.5194/acp-11-3227-2011.

(63) Lauraguais, A.; El Zein, A.; Coeur, C.; Obeid, E.; Cassez, A.; Rayez, M.-T.; Rayez, J.-C.

Kinetic Study of the Gas-Phase Reactions of Nitrate Radicals with Methoxyphenol Compounds: Experimental and Theoretical Approaches. *J. Phys. Chem. A* **2016**, *120* (17), 2691–2699. https://doi.org/10.1021/acs.jpca.6b02729.

(64) CropScape - NASS CDL Program https://nassgeodata.gmu.edu/CropScape/ (accessed Aug 6, 2018).

(65) Brown, S. Absorption Spectroscopy in High Finesse Cavities for Atmospheric Studies. *Chem. Rev.* **2003**, *103*, 5219.

(66) Brown, S. S.; Stark, H.; Ravishankara, A. R. Applicability of the Steady State Approximation to the Interpretation of Atmospheric Observations of NO 3 and N 2 O 5. *J. Geophys. Res.* **2003**, *108* (D17), 4539. https://doi.org/10.1029/2003JD003407.

(67) Olariu, R. I.; Bejan, I.; Barnes, I.; Klotz, B.; Becker, K. H.; Wirtz, K. Rate Coefficients for the Gas-Phase Reaction of NO3 Radicals with Selected Dihydroxybenzenes. *Int. J. Chem. Kinet.* **2004**, *36* (11), 577–583. https://doi.org/10.1002/kin.20029.

(68) Finewax, Z.; De Gouw, J. A.; Ziemann, P. J. Identification and Quantification of 4-Nitrocatechol Formed from OH and NO3Radical-Initiated Reactions of Catechol in Air in the Presence of NOx: Implications for Secondary Organic Aerosol Formation from Biomass Burning. *Environ. Sci. Technol.* **2018**, *52* (4), 1981–1989. https://doi.org/10.1021/acs.est.7b05864.

(69) Desyaterik, Y.; Sun, Y.; Shen, X.; Lee, T.; Wang, X.; Wang, T.; Collett, J. L. Speciation of “Brown” Carbon in Cloud Water Impacted by Agricultural Biomass Burning in Eastern China. *J. Geophys. Res. Atmos.* **2013**, *118* (13), 7389–7399. https://doi.org/10.1002/jgrd.50561.

(70) Claeys, M.; Vermeylen, R.; Yasmeen, F.; Gómez-González, Y.; Chi, X.; Maenhaut, W.; Mészáros, T.; Salma, I. Chemical Characterisation of Humic-like Substances from Urban, Rural and Tropical Biomass Burning Environments Using Liquid Chromatography with UV/Vis Photodiode Array Detection and Electrospray Ionisation Mass Spectrometry. *Environ. Chem.* **2012**, *9* (3), 273–284. https://doi.org/10.1071/EN11163.

(71) Lin, P.; Bluvshtein, N.; Rudich, Y.; Nizkorodov, S. A.; Laskin, J.; Laskin, A. Molecular Chemistry of Atmospheric Brown Carbon Inferred from a Nationwide Biomass Burning Event. *Environ. Sci. Technol.* **2017**, *51* (20), 11561–11570. https://doi.org/10.1021/acs.est.7b02276.

(72) Iinuma, Y.; Boge, O.; Grade, R.; Herrmann, H. Methyl-Nitrocatechols : Atmospheric Tracer Compounds for Biomass Burning Secondary Organic Aerosols. *Environ. Sci. Technol.* **2010**, *44*, 8453–8459.

(73) Gaston, C. J.; Lopez-Hilfiker, F. D.; Whybrew, L. E.; Hadley, O.; McNair, F.; Gao, H.; Jaffe, D. A.; Thornton, J. A. Online Molecular Characterization of Fine Particulate Matter in Port Angeles, WA: Evidence for a Major Impact from Residential Wood Smoke. *Atmos. Environ.* **2016**, *138*, 99–107. https://doi.org/10.1016/j.atmosenv.2016.05.013.

(74) Mohr, C.; Lopez-Hilfiker, F. D.; Zotter, P.; Prévoît, A. S. H.; Xu, L.; Ng, N. L.; Herndon, S. C.; Williams, L. R.; Franklin, J. P.; Zahniser, M. S.; Worsnop, D. R.; Knighton, W. B.; Aiken, A. C.; Gorkowski, K. J.; Dubey, M. K.; Allan, J. D.; Thornton, J. A. Contribution of Nitrated Phenols to Wood Burning Brown Carbon Light Absorption in Detling, United Kingdom during Winter Time. *Environ. Sci. Technol.* **2013**, *47* (12), 6316–6324. https://doi.org/10.1021/es400683v.

(75) Xie, M.; Chen, X.; Hays, M. D.; Lewandowski, M.; Offenberg, J.; Kleindienst, T. E.; Holder, A. L. Light Absorption of Secondary Organic Aerosol: Composition and Contribution of Nitroaromatic Compounds. *Environ. Sci. Technol.* **2017**, *51* (20), 11607–11616. https://doi.org/10.1021/acs.est.7b03263.

(76) Hinrichs, R. Z.; Buczek, P.; Trivedi, J. J. Solar Absorption by Aerosol-Bound Nitrophenols Compared to Aqueous and Gaseous Nitrophenols. *Environ. Sci. Technol.* **2016**, *50* (11), 5661–5667. https://doi.org/10.1021/acs.est.6b00302.

(77) Odum Jay, R.; Hoffmann, T.; Bowman, F.; Collins, D.; Flagan Richard, C.; Seinfeld John, H. Gas Particle Partitioning and Secondary Organic Aerosol Yields. *Environ. Sci. Technol.* **1996**, *30* (8), 2580–2585. https://doi.org/10.1021/es950943+.